Delocalized nonlinear vibrational modes and discrete breathers in *β*-FPUT simple cubic lattice

S. A. Shcherbinin,[1,2,*] A. M. Kazakov,[3,†] Yu. V. Bebikhov,[4,‡] A. A. Kudreyko [5,§] and S. V. Dmitriev [6,‖]

[1]*Peter the Great St. Petersburg Polytechnic University, Polytechnicheskaya St. 29, 195251, St. Petersburg, Russia*

[2]*Institute for Problems in Mechanical Engineering, Russian Academy of Sciences, V. O., Bolshoj Ave. 61, 199178, St. Petersburg, Russia*

[3]*Research Laboratory Metals and Alloys under Extreme Impacts, Ufa University of Science and Technology,*
Zaki Validi St. 32, Ufa 450076, Russia

[4]*Polytechnic Institute (Branch) in Mirny, North-Eastern Federal University, Tikhonova St. 5/1, 678170 Mirny,*
Sakha Republic (Yakutia), Russia

[5]*Bashkir State Medical University, Lenina St. 3, 450008 Ufa, Russia*

[6]*Institute of Molecule and Crystal Physics, UFRC of Russian Academy of Sciences, Oktyabrya Ave. 151, Ufa 450075, Russia*

The problem of finding various discrete breathers (DBs) in the *β*-Fermi-Pasta-Ulam-Tsingou simple cubic lattice is addressed. DBs are obtained by imposing localizing functions on delocalized nonlinear vibrational modes (DNVMs) having frequencies above the phonon spectrum of the lattice. Among 27 DNVMs with the wave vector at the boundary of the first Brillouin zone there are three satisfying this condition. Seven robust DBs of different symmetries are found using this approach.

I. INTRODUCTION

Nonlinear lattices admit localization of vibrational energy in the form of discrete breathers (DBs), also called intrinsic localized modes [1–3]. DBs have been extensively studied, mainly in low-dimensional lattices [4–8]. At the same time, most of the crystals used in practice are three-dimensional, so the study of DBs in lattices of higher dimensions is an important problem in condensed matter physics [9].

DBs in crystals are studied experimentally by measuring vibrational spectra using Raman, x-ray, and neutron scattering methods [10–13]. In addition to the signal from DBs, the spectra contain information about vibrations localized at crystal structure defects, which can overlap and make it difficult to interpret the experimental data [13]. With this in mind, computer simulation methods today remain the main tool for studying DBs in crystals. With the help of molecular dynamics, DBs were found in alkali halide crystals [14–16]; covalent crystals such as diamond, Si, and Ge [17,18]; face-centered cubic (fcc) metals [19–26], body-centered cubic (bcc) metals [19,27–29], hexagonal close-packed (hcp) metals [30,31], *α*-uranium [32], and ordered alloys [33–36]. One-dimensional [37] and two-dimensional crystals also support DBs, e.g., crystals with Morse potential [38,39], graphene [40–43], graphane (hydrogenated graphene) [44,45], and carbon nanotubes [46–49].

DBs interact with crystal structure defects [48,50,51]; they can exist at thermal equilibrium [16,38,52] and affect the properties of crystals [53–58].

Chaotic DBs are formed in the nonlinear lattices when a short-wavelength vibrational mode with frequency outside the phonon band is modulationally unstable [59]. Chaotic DBs were studied in nonlinear chains [59–66], in two-dimensional [7,60,67] and three-dimensional lattices [20].

Further progress in studying the effect of DBs on the mechanical and physical properties of crystals is impossible without knowing how many different types of DBs a particular lattice supports. In the earlier works it was shown that, for example, a two-dimensional triangular Morse lattice with an on-site harmonic potential supports breathers of two types [7], and later many more were discovered in a triangular *β*-Fermi-Pasta-Ulam-Tsingou (*β*-FPUT) lattice [68].

Recently, a practical approach has been developed to search for DBs of various symmetries in multidimensional lattices. The starting point is a search for delocalized nonlinear vibrational modes (DNVMs) that have frequencies outside the phonon spectrum. DBs are obtained by superimposing a localizing function upon such DNVMs. This approach was shown to be very efficient in finding DBs in triangular [68] and square [69] lattices, as well as in bcc metals V and Nb [27]. This approach to finding DBs is not rigorous and does not guarantee that the obtained localized solutions are single-frequency exact solutions of the equations of motion. In fact, this method detects long-lived quasi-breathers [70].

This approach is not rigorous and can be used to find long-lived quasi-DBs [70], which are not necessarily exact solutions to the equations of motion of the considered lattice.

DNVMs are found using the group-theoretical approach developed by Chechin and Sakhnenko [71]. Multidimensional lattices usually support more than one DNVM with a frequency outside the phonon band—for example, two in a square lattice [69,72], three in a triangular lattice [57,73], four in a bcc [74], and three in an fcc [75] lattice. Recently,

*stefanshcherbinin@gmail.com
†arseny.m.kazakov@gmail.com
‡bebikhov.yura@mail.ru
§alexkudreyko@mail.ru
‖dmitriev.sergey.v@gmail.com

DNVMs were applied to verify the accuracy of molecular dynamics interatomic potentials [76].

An introduction to the method of finding DNVMs developed by Chechin and Sakhnenko was given in the appendices to Ref. [73]. Their approach was used in Refs. [77–81]. Note that in the original papers, the authors spoke of bushes of nonlinear normal modes (BNNMs), and later in some papers they were called DNVMs.

The search for DBs in a simple cubic lattice is motivated by the fact that there is one metal with such a lattice, namely, polonium [82–85]. Also, the simple cubic lattice is the simplest three-dimensional lattice that can be used to test various ideas [86].

The paper is organized as follows: the model is presented in Sec. II, the phonon dispersion relation is derived in Sec. III, DNVMs with wave vectors at the boundary of the first Brillouin zone are described in Sec. IV, and in Sec. V DBs of a simple cubic lattice are obtained. A summary of this study is presented in Sec. VI.

II. SIMPLE CUBIC β-FPUT LATTICE

A three-dimensional simple cubic β-FPUT lattice is considered taking into account nearest and next-nearest interactions, see Fig. 1(a). The lattice with the step h is a set of points having radius vectors

$$\boldsymbol{\xi}_{i,j,k} = i\boldsymbol{e}_1 + j\boldsymbol{e}_2 + k\boldsymbol{e}_3, \tag{1}$$

where i, j, and k are integers and the basis vectors of the lattice are $\boldsymbol{e}_1 = (h, 0, 0)$, $\boldsymbol{e}_2 = (0, h, 0)$, and $\boldsymbol{e}_3 = (0, 0, h)$.

The atoms of mass m occupy the lattice points. Vector $\boldsymbol{\delta}_{i,j,k} = (u_{i,j,k}, v_{i,j,k}, w_{i,j,k})$ describes the displacement of the atom i, j, k from its lattice position so that the radius vector of the atom at time t is $\boldsymbol{r}_{i,j,k}(t) = \boldsymbol{\xi}_{i,j,k} + \boldsymbol{\delta}_{i,j,k}(t)$.

The interaction between nearest (n) and next-nearest (nn) neighbors is described by the β-FPUT potential

$$\varphi_{n,nn}(r) = \frac{c_{n,nn}}{2}(r - a_{n,nn})^2 + \frac{\beta_{n,nn}}{4}(r - a_{n,nn})^4, \tag{2}$$

where r is the distance between atoms; $a_n = h$ and $a_{nn} = h\sqrt{2}$ are the equilibrium lengths of the nearest and next-nearest bonds, respectively; and c_n and c_{nn} (β_n and β_{nn}) are the coefficients of the harmonic (anharmonic) part of the potential for the nearest and next-nearest bonds, respectively. We set $h = 1$ and $c_n = 1$ by normalizing the distance and energy units, respectively. For the stiffness of the next-nearest bonds two values are considered, $c_{nn} = 1$ and 3. Setting $\beta_n = \beta_{nn} = 10$ ensures that the nonlinearity becomes noticeable for atomic displacements of the order of $h/10$. The particle mass $m = 1$ is set by normalization of the time unit.

The reciprocal lattice of a simple cubic lattice is shown in Fig. 1(b) in the space of wave numbers q, s, p. Letters designate highly symmetrical points and lines of the first Brillouin zone.

The computational cell of $I \times J \times K$ atoms is considered and the periodic boundary conditions, $\boldsymbol{r}_{i,j,k} = \boldsymbol{r}_{i+I,j,k} = \boldsymbol{r}_{i,j+J,k} = \boldsymbol{r}_{i,j,k+K}$, are used.

The Hamiltonian of the computational cell is the sum of the kinetic energies of atoms and potential energies of the nearest
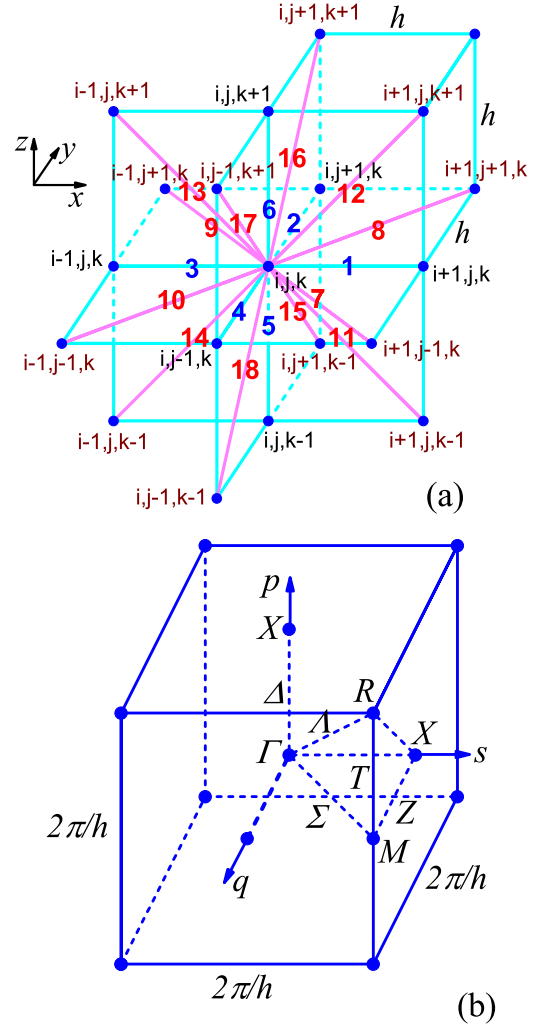

(a)

(b)

FIG. 1. (a) Simple cubic lattice with lattice parameter h. The lattice points are numbered by indices i, j, k; nearest and next-nearest bonds are colored cyan and magenta, respectively, and numbered with blue and red numbers, respectively. (b) Reciprocal lattice in the space of wave numbers q, s, p. Highly symmetrical points and lines of the first Brillouin zone are designated. Line Δ connects points Γ and X; line Σ connects points Γ and M; line Λ connects points Γ and R; line T connects points M and R; and line Z connects points X and M.

and next-nearest bonds:

$$H = K + P_n + P_{nn} = \sum_{i=1}^{I}\sum_{j=1}^{J}\sum_{k=1}^{K}\frac{m}{2}|\dot{\boldsymbol{r}}_{i,j,k}|^2$$

$$+ \frac{1}{2}\sum_{i=1}^{I}\sum_{j=1}^{J}\sum_{k=1}^{K}\left(\sum_{s=1}^{6}\varphi_n(|\boldsymbol{R}_{i,j,k,s}|) + \sum_{l=7}^{18}\varphi_{nn}(|\boldsymbol{R}_{i,j,k,l}|)\right), \tag{3}$$

where the overdot denotes differentiation with respect to time and vectors connecting the six nearest ($\boldsymbol{R}_{i,j,k,s}$) and 12 next-nearest ($\boldsymbol{R}_{i,j,k,l}$) neighbors of the i, j, k particle are defined by Eq. (A1).

The equations of motion of the i, j, k atom derived from Eq. (3) are

$$m\ddot{u}_{i,j,k} = \sum_{s=1}^{6} D_n R_{i,j,k,s,x} + \sum_{l=7}^{18} D_{nn} R_{i,j,k,l,x},$$

$$m\ddot{v}_{i,j,k} = \sum_{s=1}^{6} D_n R_{i,j,k,s,y} + \sum_{l=7}^{18} D_{nn} R_{i,j,k,l,y},$$

$$m\ddot{w}_{i,j,k} = \sum_{s=1}^{6} D_n R_{i,j,k,s,z} + \sum_{l=7}^{18} D_{nn} R_{i,j,k,l,z}, \quad (4)$$

where

$$D_n = \frac{\varphi'_n(|\mathbf{R}_{i,j,k,s}|)}{|\mathbf{R}_{i,j,k,s}|}, \quad D_{nn} = \frac{\varphi'_{nn}(|\mathbf{R}_{i,j,k,l}|)}{|\mathbf{R}_{i,j,k,l}|}. \quad (5)$$

The dynamics of DNVMs is analyzed using the computational cell with $I = J = K = 4$, which is sufficient for all considered modes due to their spatial periodicity. DBs are studied in the computational cell with $I = J = K = 40$, which is sufficient due to their spatial localization.

In the analysis of DBs, absorbing boundary conditions are used to damp low-amplitude waves emitted by the DB when reaching a stationary dynamic regime.

The numerical integration of the equations of motion is carried out by the symplectic Störmer method of the sixth order [87] with a time step of 0.01, which is sufficient to preserve the total energy with a relative error not exceeding 10^{-6} during the entire numerical run.

III. PHONON DISPERSION RELATION

In the Appendix, the cubic characteristic equation Eq. (A9) is derived from the linearized equations of motion Eqs. (A2)–(A4). The characteristic equation relates the frequencies of the three branches of the dispersion relation with the wave numbers q, s, and p.

Let us consider dispersion relations along the four high-symmetry lines in the reciprocal space, see Fig. 1(b).

For Λ line $q = s = p$ and the dispersion relations obtain the form

$$m\omega_1^2 = 4c_n \sin^2 \frac{q}{2} + 8c_{nn} \sin^2 q,$$

$$m\omega_{2,3}^2 = 4c_n \sin^2 \frac{q}{2} + 2c_{nn} \sin^2 q. \quad (6)$$

For Σ line $q = s$, $p = 0$, and one gets

$$m\omega_1^2 = 8c_{nn} \sin^2 \frac{q}{2},$$

$$m\omega_2^2 = (4c_n + 4c_{nn}) \sin^2 \frac{q}{2},$$

$$m\omega_3^2 = (4c_n + 4c_{nn}) \sin^2 \frac{q}{2} + 4c_{nn} \sin^2 q. \quad (7)$$

For Δ line $s = p = 0$, which leads to

$$m\omega_1^2 = (4c_n + 8c_{nn}) \sin^2 \frac{q}{2},$$

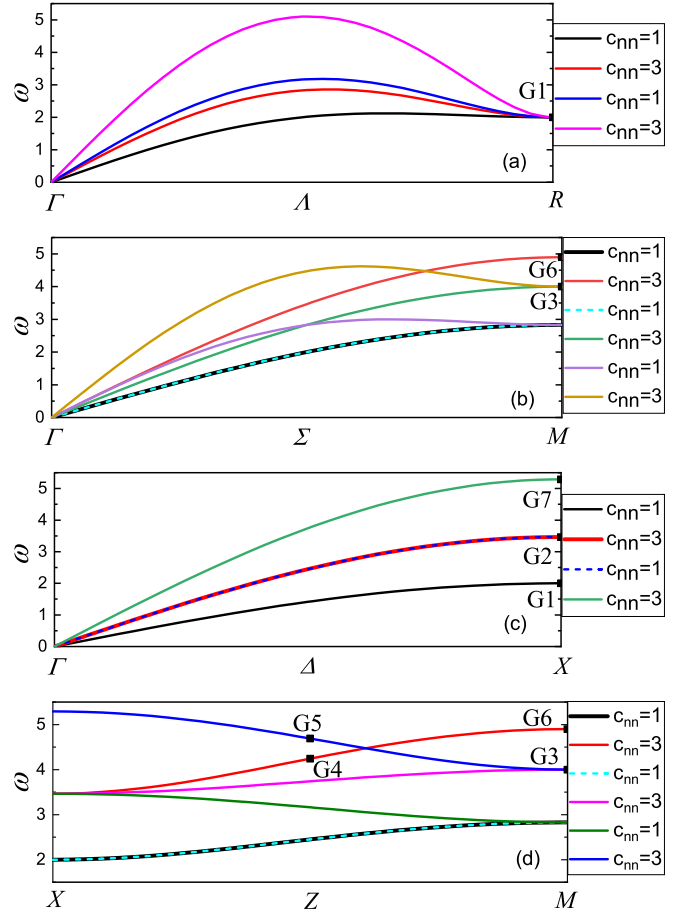$$m\omega_{2,3}^2 = 4c_{nn} \sin^2 \frac{q}{2}. \quad (8)$$

FIG. 2. Dispersion curves of the simple cubic lattice for the highly symmetrical lines of the first Brillouin zone. (a) Λ line, see Eq. (6); (b) Σ line, see Eq. (7); (c) Δ line, see Eq. (8); (d) Z line, see Eq. (9). Results for $c_{nn} = 1$ and $c_{nn} = 3$ are compared while $c_n = 1$ for all cases. Black squares show the frequencies of the phonons of seven groups of DNVMs in the small-amplitude limit.

For Z line $p = 0$, $s = \pi/h$ and the dispersion relations are

$$m\omega_1^2 = 4c_{nn} + 4c_{nn} \sin^2 \frac{q}{2},$$

$$m\omega_2^2 = (4c_n + 4c_{nn}) \sin^2 \frac{q}{2} + 4c_{nn} \sin^2 \frac{q - \pi}{2},$$

$$m\omega_3^2 = 4c_n + 4c_{nn} + 4c_{nn} \sin^2 \frac{q - \pi}{2}. \quad (9)$$

In Fig. 2, the dispersion relations for the high-symmetry lines in the first Brillouin zone are plotted.

For point M the frequency is equal to

$$\omega_M^2 = 8c_{nn}, \quad (10)$$

and for point X the frequency is equal to

$$\omega_X^2 = 4c_n + 8c_{nn}. \quad (11)$$

The frequency at point X is higher than the frequency at point M for any values of $c_n > 0$ and c_{nn}. We conclude that the maximum phonon frequency is

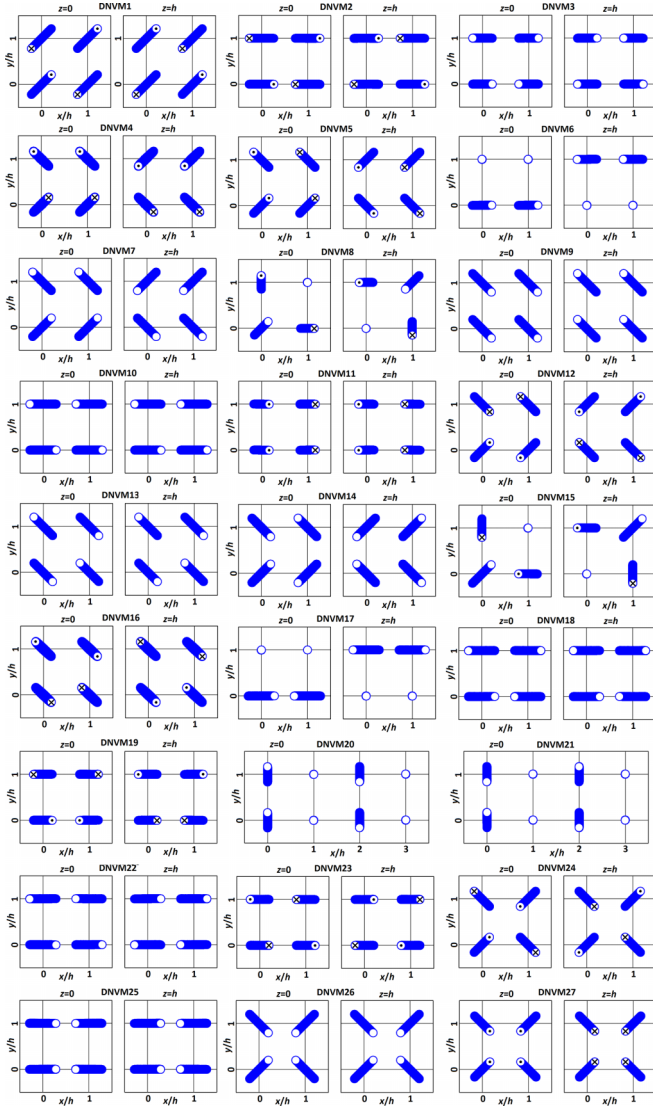$$\omega_{\max} = \omega_X = 2\sqrt{c_n + 2c_{nn}}. \quad (12)$$

FIG. 3. Zone boundary DNVMs of a simple cubic lattice. Atomic trajectories are shown in blue. The circles show the atoms at the moment of the greatest deviation from the position in the lattice. An empty circle means zero z displacement, while dots and crosses correspond to positive and negative z displacements, respectively. All nonzero displacement components are equal to each other.

IV. ZONE BOUNDARY DNVMS OF SIMPLE CUBIC LATTICE

There are 27 one-component DNVMs of a simple cubic lattice with wave vectors at the boundary of the first Brillouin zone; they are shown in Fig. 3. The method of deriving DNVMs has been reported in the Appendix of Ref. [72]. All these vibrational modes are dynamical systems with one degree of freedom. Thick blue lines show the trajectories of atoms projected onto the xy plane. The white circles show the positions of the atoms at the moment of their maximum displacement from the lattice sites. Empty circles mean that the z component of displacement is equal to zero. Circles with dots and crosses are used to denote the positive and negative z components of the displacement, respectively. It is important to note that all nonzero components of initial
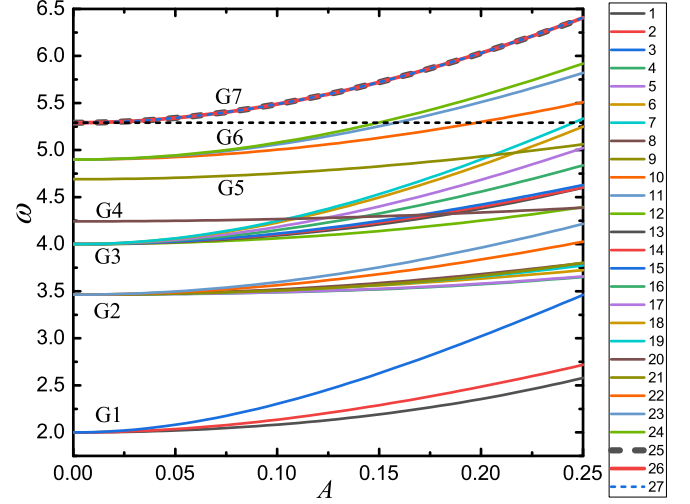

FIG. 4. Frequency as the function of amplitude for 27 DNVMs for $c_n = 1$ and $c_{nn} = 3$. The upper edge of the phonon spectrum, $\omega_{\max} = 2\sqrt{7} = 5.29$, is shown by the horizontal dashed line. All DNVMs are divided into seven groups labeled G1–G7 according to the frequency Ω in the small-amplitude limit, see Table I. The DNVMs are ordered according to their frequencies, and the higher numbered mode has the higher frequency. DNVMs of group G7 have frequencies above the phonon spectrum for all amplitudes.

atomic displacements are equal in magnitude. For example, for DNVM1 $|u_{i,j,k}^0| = |v_{i,j,k}^0| = |w_{i,j,k}^0| > 0$, for DNVM2 $|u_{i,j,k}^0| = |w_{i,j,k}^0| > 0$, $|v_{i,j,k}^0| = 0$, for DNVM3 $|u_{i,j,k}^0| > 0$, $|w_{i,j,k}^0| = |v_{i,j,k}^0| = 0$, and so on.

For most DNVMs, atomic displacements are shown in Fig. 3 for a translational cell containing $2 \times 2 \times 2$ primitive cubic cells, or eight atoms. For each DNVM, the displacements are shown for two planes, $z = 0$ and $z = h$. The two exceptions are DNVM20 and DNVM21; they have rectangular translation cells with $4 \times 2 \times 1$ atoms and it is sufficient to show only the $z = 0$ plane.

In DNVMs 6, 8, 15, 17, 20, and 22 there are atoms with zero initial displacement, and they remain at rest while initially displaced atoms oscillate.

In Fig. 4, the frequency response of 27 DNVMs is shown for $c_n = 1$ and $c_{nn} = 3$. The upper edge of the phonon spectrum is shown as a horizontal dashed line, $\omega_{\max} = 2\sqrt{7} = 5.29$, see Eq. (12).

In Fig. 5, similar results are shown for $c_n = c_{nn} = 1$. The upper edge of the phonon spectrum is shown as a horizontal dashed line, $\omega_{\max} = 2\sqrt{3} = 3.46$, see Eq. (12).

TABLE I. DNVMs separated into groups according to their frequency Ω in the small-amplitude limit. Results for $c_n = 1$, $c_{nn} = 3$.

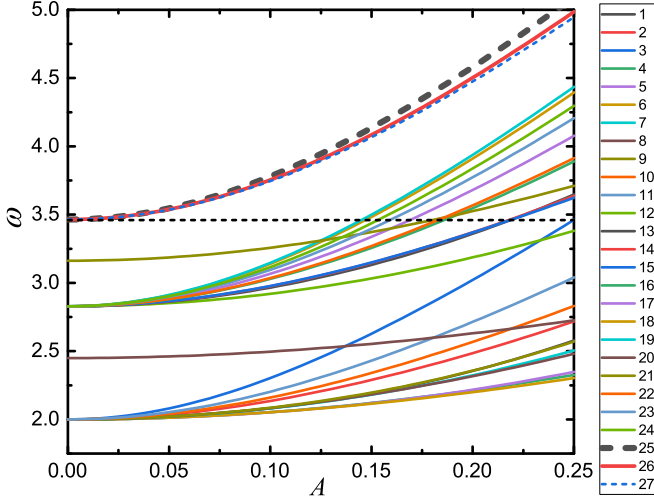| Group	G1	G2	G3	G4
DNVMs	1–3	4–11	12–19	20
Ω	2.00	3.46	4.00	4.24
Group	G5	G6	G7	
DNVMs	21	22-24	25–27	
Ω	4.69	4.90	5.29	

FIG. 5. Frequency as the function of amplitude for 27 DNVMs for $c_n = c_{nn} = 1$. The upper edge of the phonon spectrum, $\omega_{\max} = 2\sqrt{3} = 3.46$, is shown by the horizontal dashed line. DNVMs from 25 to 27 have frequencies above the phonon spectrum for all amplitudes, the same as in Fig. 4.

It can be seen from Fig. 4 that DNVMs can be divided into seven groups, designated from G1 to G7, according to the frequency in the limit of small amplitudes, when DNVMs are transformed into zone-boundary phonons. Table I shows the division of DNVMs into groups and the mode frequencies in the limit of small amplitudes for $c_n = 1$, $c_{nn} = 3$. These frequencies are also shown in Fig. 2 by black squares. In Fig. 5, some groups are combined due to a special choice of model parameters, namely, $c_n = c_{nn} = 1$.

V. DISCRETE BREATHERS

As mentioned above, here we aim to find long-lived quasi-DBs [70], which are not necessarily exact solutions of the equations of motion of the simple cubic lattice. For brevity, quasi-DBs will be called DBs.

DBs are obtained below by superimposing the localizing functions on the DNVMs with frequencies above the phonon spectrum, i.e., on DNVM25, DNVM26, and DNVM27; they belong to group G7.

The DB is localized at the point of intersection of three orthogonal planes,

$$L_1 x + L_2 y + L_3 z + L_4 = 0, \tag{13}$$

$$M_1 x + M_2 y + M_3 z + M_4 = 0, \tag{14}$$

$$N_1 x + N_2 y + N_3 z + N_4 = 0, \tag{15}$$

and the conditions of their orthogonality are

$$L_1 M_1 + L_2 M_2 + L_3 M_3 = 0, \tag{16}$$

$$L_1 N_1 + L_2 N_2 + L_3 N_3 = 0, \tag{17}$$

$$M_1 N_1 + M_2 N_2 + M_3 N_3 = 0. \tag{18}$$

The localizing function is taken in the form

$$a_{ijk} = \frac{A}{\cosh(\gamma_1 d_{ijk}) \cosh(\gamma_2 f_{ijk}) \cosh(\gamma_3 g_{ijk})}, \tag{19}$$

where a_{ijk} is the magnitude of the initial displacement of particle with the lattice position $\boldsymbol{\xi}_{i,j,k}$; A is the DNVM amplitude; γ_1, γ_2, and γ_3 are the localization parameters; and d_{ijk}, f_{ijk}, and g_{ijk} are the distances from the lattice point i, j, k to the planes Eqs. (13)–(15), respectively, which are calculated as

$$d_{ijk} = \frac{|L_1 x_{ijk} + L_2 y_{ijk} + L_3 z_{ijk} + L_4|}{\sqrt{L_1^2 + L_2^2 + L_3^2}}, \tag{20}$$

$$f_{ijk} = \frac{|M_1 x_{ijk} + M_2 y_{ijk} + M_3 z_{ijk} + M_4|}{\sqrt{M_1^2 + M_2^2 + M_3^2}}, \tag{21}$$

$$g_{ijk} = \frac{|N_1 x_{ijk} + N_2 y_{ijk} + N_3 z_{ijk} + N_4|}{\sqrt{N_1^2 + N_2^2 + N_3^2}}. \tag{22}$$

Initial velocities of all particles are equal to zero for all types of DBs.

In short, according to Eq. (19), the value of the initial displacements of atoms, a_{ijk}, decays exponentially with distance from each of the three orthogonal planes Eqs. (13)–(15).

The strategy of quasi-DB search is very simple. All quasi-DBs are obtained at the intersection of three orthogonal planes,

$$x + L_4 = 0, \tag{23}$$

$$y + M_4 = 0, \tag{24}$$

$$z + N_4 = 0. \tag{25}$$

That is, in Eqs. (13)–(15) $L_1 = M_2 = N_3 = 1$ and $L_2 = L_3 = M_1 = M_3 = N_1 = N_2 = 0$. The orthogonality conditions Eqs. (16)–(18) are met. Parameters L_4, M_4, and N_4 define the localization center relative to the lattice nodes. The choice of localization parameters is not optimized. For typical values of $A = 0.2$ and $\gamma_1 = \gamma_2 = \gamma_3 = 1$, the ansatz Eq. (19) usually gives a localized vibrational mode, which, after the emission of some part of the initial energy, is transformed into a quasi-DB with a very long lifetime. The time required to stabilize the quasi-DB is denoted as t^*. Typically, t^* is between 15 and 30 oscillation periods, which corresponds to about 20–40 time units. The energy emitted by the DB during stabilization is absorbed at the boundaries of the computational cell.

In all cases the model parameters are $c_n = c_{nn} = 1$, $\beta_n = \beta_{nn} = 10$, and $m = 1$.

A. DBs based on DNVM 25

In Fig. 6(a), the DB based on DNVM25 localized at the intersection of the $x = 0$, $y = 0$, and $z = 0$ planes is shown. Thus, in Eqs. (23)–(25) $L_4 = M_4 = N_4 = 0$. Parameters of the localization function Eq. (19) are $A = 0.2$, $\gamma_1 = 0.8$ and $\gamma_2 = \gamma_3 = 1.0$. Atomic trajectories are shown projected onto the xy, xz, and yz planes. Atoms are shown at the moment of maximum deviation from their lattice positions. This on-site DB has one atom vibrating with the largest amplitude. In Fig. 6(b), the displacement u_{ijk} for the atom colored red is
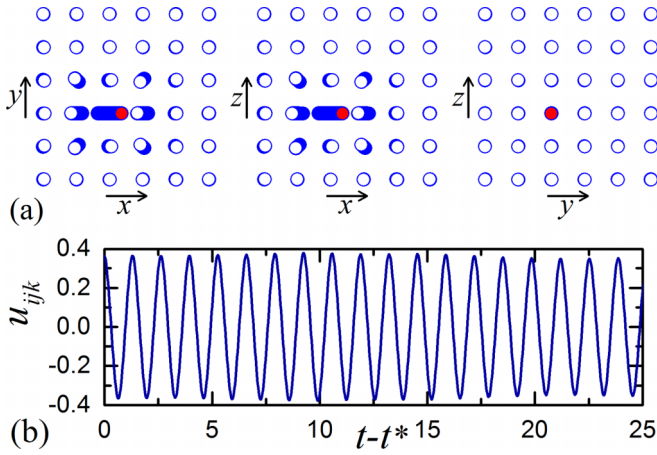
FIG. 6. (a) DB based on DNVM25 localized at the intersection of the $x = 0$, $y = 0$, and $z = 0$ planes. Atomic trajectories are shown in projections onto the xy, xz, and yz planes. (b) Displacement u_{ijk} of the atom colored red as a function of time for $t > t^*$.

plotted as the function of time for $t > t^*$, where t^* is the time needed for stabilization of the DB.

In Fig. 7(a), the DB based on DNVM25 localized at the intersection of the $x = h/2$, $y = 0$, and $z = 0$ planes is shown. In Eqs. (23)–(25), $L_4 = -h/2$ and $M_4 = N_4 = 0$. Parameters of the localization function Eq. (19) are $A = 0.2$, $\gamma_1 = 0.8$, and $\gamma_2 = \gamma_3 = 1.0$. This intersite DB has two atoms vibrating with the largest amplitude. In Fig. 7(b), the displacement u_{ijk} for the atom colored red is plotted as the function of time for $t > t^*$.

B. DBs based on DNVM 26

In Figs. 8–10, DBs based on DNVM 26 are presented. In Figs. 8(a), 9(a), and 10(a), trajectories of atoms are shown projected onto the xy, xz, and yz planes. The atoms are shown at the time of maximum deviation from the lattice positions.
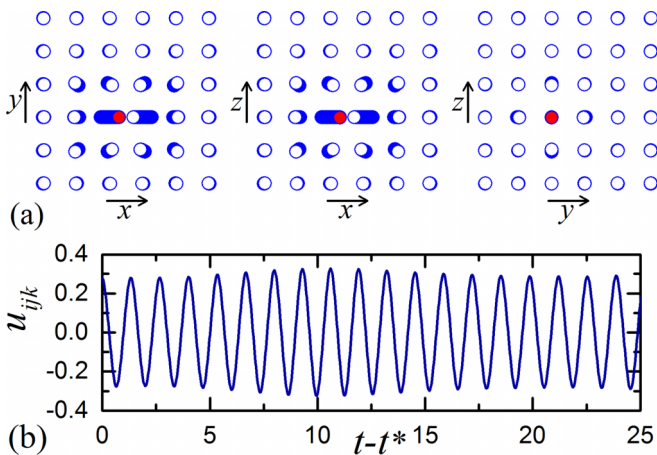

FIG. 7. (a) DB based on DNVM25 localized at the intersection of the $x = h/2$, $y = 0$, and $z = 0$ planes. Atomic trajectories are shown in projections onto the xy, xz, and yz planes. (b) Displacement u_{ijk} of the atom colored red as a function of time for $t > t^*$.
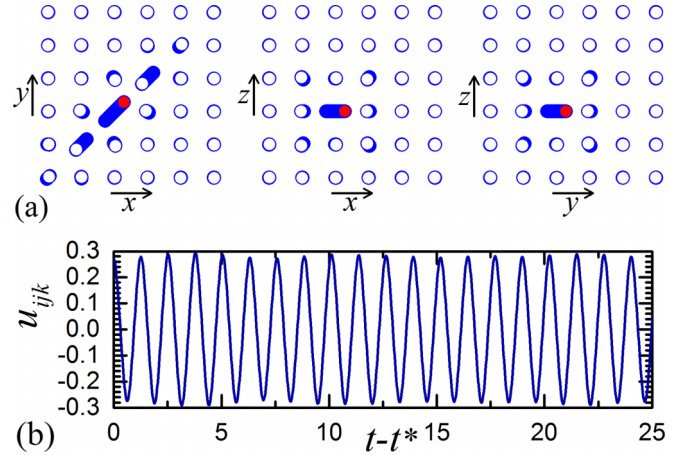

FIG. 8. (a) DB based on DNVM26 localized on the intersection of the planes $x = 0$, $y = 0$, and $z = 0$. Displacements of atoms are shown projected onto the xy, xz, and yz planes. (b) Displacement u_{ijk} of the atom colored red as the function of time for $t > t^*$.

In Figs. 8(b), 9(b), and 10(b), displacement u_{ijk} of the atom colored red is plotted as the function of time for $t > t^*$.

In Fig. 8, the DB is localized at the intersection of the planes $x = 0$, $y = 0$, and $z = 0$. Parameters of the localization function Eq. (19) are $A = 0.2$, $\gamma_1 = \gamma_2 = \gamma_3 = 1.0$. This on-site DB has one atom vibrating with the largest amplitude.

In Fig. 9, the DB is localized on the intersection of the planes $x = 0$, $y = 0$, and $z = h/2$. Parameters of the localization function Eq. (19) are $A = 0.24$, $\gamma_1 = \gamma_2 = \gamma_3 = 1.0$. For this DB two atoms have the largest vibration amplitude.

In Fig. 10, the DB is localized on the intersection of the planes $x = h/2$, $y = h/2$, and $z = 0$. Parameters of the localization function Eq. (19) are $A = 0.2$, $\gamma_1 = \gamma_2 = \gamma_3 = 1.0$. For this DB four atoms have the largest vibration amplitude.
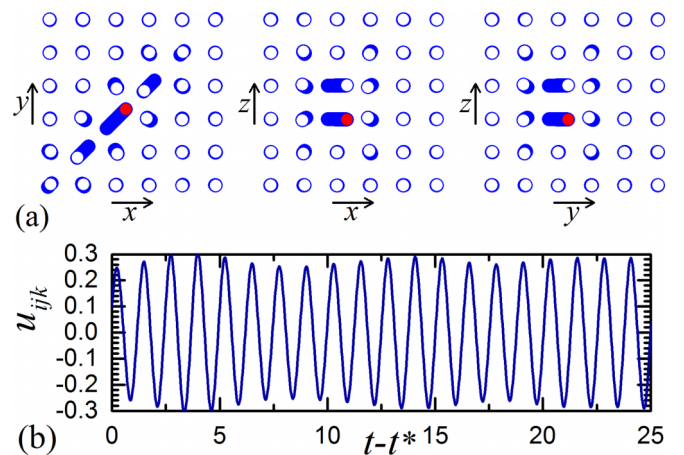

FIG. 9. (a) DB based on DNVM26 localized on the intersection of the planes $x = 0$, $y = 0$, and $z = h/2$. Displacements of atoms are shown projected onto the xy, xz, and yz planes. (b) Displacement u_{ijk} of the atom colored red as the function of time for $t > t^*$.
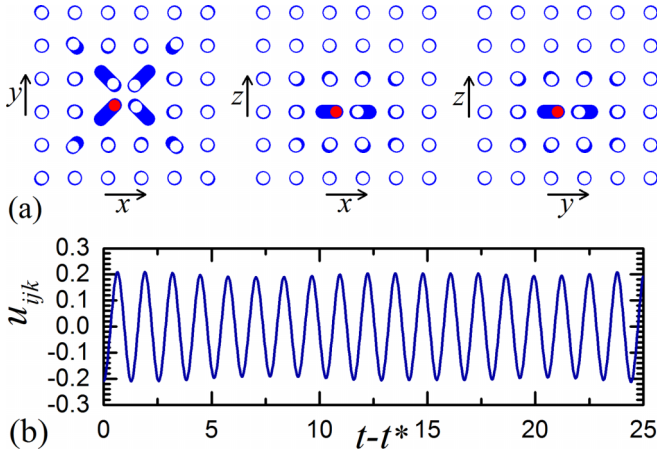
FIG. 10. (a) DB based on DNVM26 localized on the intersection of the planes $x = h/2$, $y = h/2$, and $z = 0$. Displacements of atoms are shown projected onto the xy, xz, and yz planes. (b) Displacement u_{ijk} of the atom colored red as the function of time for $t > t^*$.

C. DBs based on DNVM 27

In Figs. 11 and 12, DBs based on DNVM 27 are presented similarly to the other DBs.

In Fig. 11, the DB is localized at the intersection of the planes $x = h/2$, $y = h/2$, and $z = h/2$. Parameters of the localization function Eq. (19) are $A = 0.22$, $\gamma_1 = \gamma_2 = \gamma_3 = 1.2$. This intersite DB has eight atoms vibrating with the largest amplitude.

In Fig. 12, the DB is localized on the intersection of the planes $x = 0$, $y = 0$, and $z = 0$. Parameters of the localization function Eq. (19) are $A = 0.22$, $\gamma_1 = \gamma_2 = \gamma_3 = 1.2$. For this on-site DB one atom has the largest vibration amplitude.

VI. DISCUSSION AND CONCLUSIONS

In this study, 27 zone-boundary DNVMs of the simple cubic lattice were obtained (see Fig. 3) using the group-theoretical approach according to Chechin and Sakhnenko
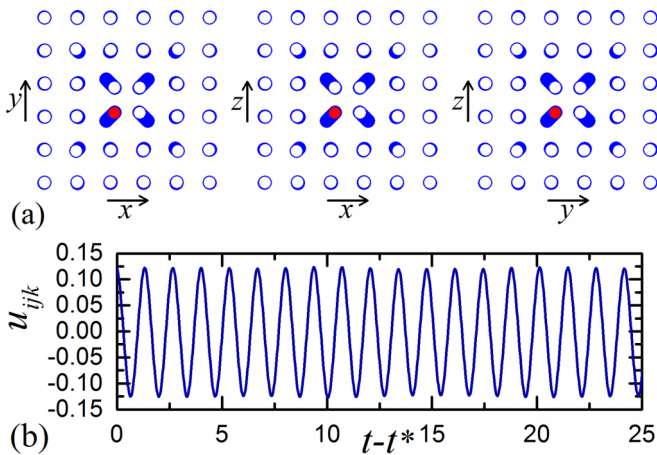

FIG. 11. (a) DB based on DNVM27 localized on the intersection of the planes $x = h/2$, $y = h/2$, and $z = h/2$. Displacements of atoms are shown projected onto the xy, xz, and yz planes. (b) Displacement u_{ijk} of the atom colored red as the function of time for $t > t^*$.
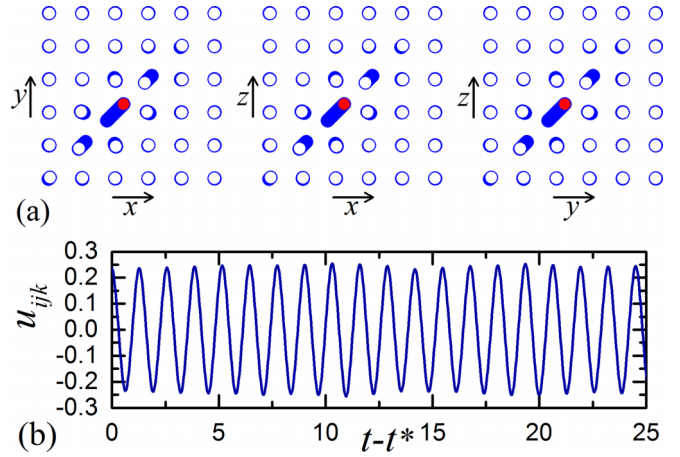

FIG. 12. (a) DB based on DNVM27 localized on the intersection of the planes $x = 0$, $y = 0$, and $z = 0$. Displacements of atoms are shown projected onto the xy, xz, and yz planes. (b) Displacement u_{ijk} of the atom colored red as the function of time for $t > t^*$.

[71]. We limited ourselves to consideration of only zone-boundary modes, since we are looking for DNVMs that have a frequency above the phonon spectrum for all vibration amplitudes, and such modes should have a wave vector at the boundary of the first Brillouin zone.

In the small-amplitude limit, DNVMs transform into the zone-boundary phonon modes, but even at large amplitudes they retain the oscillation pattern and do not excite other modes, making them special among the ordinary phonons that begin to interact with other modes at large oscillation amplitudes. This special property of the DNVMs is guaranteed by the symmetry of the lattice. It is important to note that the DNVMs shown in Fig. 3 exist as exact solutions in a simple cubic lattice with any type of interatomic interaction, since only the symmetry of the lattice was taken into account in their derivation. In particular, all 27 DNVMs exist as exact nonlinear solutions in the simple cubic lattice of polonium, as guaranteed by the lattice symmetry.

The properties of DNVMs depend on the choice of inter-particle potentials. Any type of potential can be considered, including first-principles simulations [74], but for the first study of DNVMs in a simple cubic lattice, the classical β-FPUT potential was chosen, which does not include the cubic anharmonicity in the potential energy. The introduction of the cubic term could lead to a softening of the potential and less favorable conditions for the existence of DBs in the lattice. Our second important goal is to establish the relationship between DNVMs and DBs, and this justifies the use of the β-FPUT potential for demonstration purposes.

The frequency response of the DNVMs was obtained, see Figs. 4 and 5. Three DNVMs have frequencies above the phonon band for any amplitude, namely, DNVM25, DNVM26, and DNVM27. These modes in the small-amplitude limit reduce to the phonons with the wave vector at point X of the first Brillouin zone, see Fig. 1(b).

Seven robust quasi-DBs were obtained by applying the localization function Eq. (19) to three DNVMs with frequencies above the phonon spectrum, see Figs. 6–12. The parameters of the localization function were not optimized, since the

purpose of this study is only to demonstrate the simplicity of obtaining quasi-DBs by the proposed method. The problem of finding multiple solutions to the nonlinear equations of motion does not have a general solution. However, in this work we were able to find quasi-DBs of different symmetry. An alternative approach for analyzing the multiplicity of solutions is the numerical continuation [88–91], a method for tracking families of solutions of a nonlinear system as a function of some parameter.

It is important to discuss the effect of the on-site potential. There is no such potential in crystals, but it is often used in theoretical discrete nonlinear models. The introduction of an on-site potential produces a low-frequency gap in the phonon spectrum. At the same time, a new DNVM appears in the form when all particles move synchronously in the on-site potential. If the on-site potential has a soft-type anharmonicity, the frequency of this DNVM will decrease with the amplitude and enter the gap. Then, by applying a localizing function, one can try to obtain a DB in accordance with the approach offered in this work.

The quasi-DBs obtained in this study can be used as initial conditions for finding time-periodic exact DBs, if they are supported by the considered lattice. We have not done so, since the purpose of our study is to show the relationship between the delocalized and spatially localized long-lived vibrational modes.

As can be seen from Figs. 4 and 5, the frequencies of some DNVMs are within the phonon spectrum at low amplitudes and rise above the spectrum as the amplitude increases. Interestingly, in some cases, DBs can be obtained based on such DNVMs [27]. We do not analyze such DBs here, since they can exist only at large amplitudes.

An important issue is the effect of perturbations such as thermal oscillations on the dynamics of DNVMs and DBs. Typically, at amplitudes above the threshold, DNVMs become modulationally unstable and are destroyed even in the presence of very small perturbations. If the DNVM frequency is outside the phonon spectrum, its energy cannot be directly given to the extended phonons and the modulational instability leads to the formation of chaotic DBs [20,57]. As for DBs, they are also affected by the thermal fluctuations, but in a different way. On the one hand, fluctuations limit the lifetime of DBs, but on the other hand, they produce thermally populated DBs [13,16,38].

In further work, DNVMs and DBs in other lattices will be obtained using the approach presented here. In particular, DNVMs in body-centered cubic lattice of tungsten were recently studied by molecular dynamics and *ab initio* methods [74]. The ultimate goal of these studies is to analyze the role of DBs in solid state physics.

The data that support the findings of this study are available on request from the corresponding author, S.V.D.

APPENDIX

Referring to Fig. 1(a), the following vectors connecting the six nearest and twelve next-nearest neighbors of the i, j, k particle are defined:

$$\boldsymbol{R}_{i,j,k,1} = \boldsymbol{r}_{i+1,j,k} - \boldsymbol{r}_{i,j,k},$$
$$\boldsymbol{R}_{i,j,k,2} = \boldsymbol{r}_{i,j+1,k} - \boldsymbol{r}_{i,j,k},$$
$$\boldsymbol{R}_{i,j,k,3} = \boldsymbol{r}_{i-1,j,k} - \boldsymbol{r}_{i,j,k},$$
$$\boldsymbol{R}_{i,j,k,4} = \boldsymbol{r}_{i,j-1,k} - \boldsymbol{r}_{i,j,k},$$
$$\boldsymbol{R}_{i,j,k,5} = \boldsymbol{r}_{i,j,k-1} - \boldsymbol{r}_{i,j,k},$$
$$\boldsymbol{R}_{i,j,k,6} = \boldsymbol{r}_{i,j,k+1} - \boldsymbol{r}_{i,j,k},$$
$$\boldsymbol{R}_{i,j,k,7} = \boldsymbol{r}_{i+1,j-1,k} - \boldsymbol{r}_{i,j,k},$$
$$\boldsymbol{R}_{i,j,k,8} = \boldsymbol{r}_{i+1,j+1,k} - \boldsymbol{r}_{i,j,k},$$
$$\boldsymbol{R}_{i,j,k,9} = \boldsymbol{r}_{i-1,j+1,k} - \boldsymbol{r}_{i,j,k},$$
$$\boldsymbol{R}_{i,j,k,10} = \boldsymbol{r}_{i-1,j-1,k} - \boldsymbol{r}_{i,j,k},$$
$$\boldsymbol{R}_{i,j,k,11} = \boldsymbol{r}_{i+1,j,k-1} - \boldsymbol{r}_{i,j,k},$$
$$\boldsymbol{R}_{i,j,k,12} = \boldsymbol{r}_{i+1,j,k+1} - \boldsymbol{r}_{i,j,k},$$
$$\boldsymbol{R}_{i,j,k,13} = \boldsymbol{r}_{i-1,j,k+1} - \boldsymbol{r}_{i,j,k},$$
$$\boldsymbol{R}_{i,j,k,14} = \boldsymbol{r}_{i-1,j,k-1} - \boldsymbol{r}_{i,j,k},$$
$$\boldsymbol{R}_{i,j,k,15} = \boldsymbol{r}_{i,j+1,k-1} - \boldsymbol{r}_{i,j,k},$$
$$\boldsymbol{R}_{i,j,k,16} = \boldsymbol{r}_{i,j+1,k+1} - \boldsymbol{r}_{i,j,k},$$
$$\boldsymbol{R}_{i,j,k,17} = \boldsymbol{r}_{i,j-1,k+1} - \boldsymbol{r}_{i,j,k},$$
$$\boldsymbol{R}_{i,j,k,18} = \boldsymbol{r}_{i,j-1,k-1} - \boldsymbol{r}_{i,j,k}. \tag{A1}$$

For small displacements of atoms from their positions in the lattice, $|\boldsymbol{\delta}_{i,j,k}| \ll h$, the equations of motion Eq. (4) can be linearized as follows:

$$
\begin{aligned}
m\ddot{u}_{i,j,k} = {} & c_n(u_{i+1,j,k} - 2u_{i,j,k} + u_{i-1,j,k}) \\
& + \frac{c_{nn}}{2}(u_{i+1,j-1,k} - 2u_{i,j,k} + u_{i-1,j+1,k}) \\
& - \frac{c_{nn}}{2}(v_{i+1,j-1,k} - 2v_{i,j,k} + v_{i-1,j+1,k}) \\
& + \frac{c_{nn}}{2}(u_{i+1,j+1,k} - 2u_{i,j,k} + u_{i-1,j-1,k}) \\
& + \frac{c_{nn}}{2}(v_{i+1,j+1,k} - 2v_{i,j,k} + v_{i-1,j-1,k}) \\
& + \frac{c_{nn}}{2}(u_{i+1,j,k-1} - 2u_{i,j,k} + u_{i-1,j,k+1}) \\
& - \frac{c_{nn}}{2}(w_{i+1,j,k-1} - 2w_{i,j,k} + w_{i-1,j,k+1}) \\
& + \frac{c_{nn}}{2}(u_{i+1,j,k+1} - 2u_{i,j,k} + u_{i-1,j,k-1}) \\
& + \frac{c_{nn}}{2}(w_{i+1,j,k+1} - 2w_{i,j,k} + w_{i-1,j,k-1}), \tag{A2}
\end{aligned}
$$

$$
\begin{aligned}
m\ddot{v}_{i,j,k} = {} & c_n(v_{i,j+1,k} - 2v_{i,j,k} + v_{i,j-1,k}) \\
& - \frac{c_{nn}}{2}(u_{i+1,j-1,k} - 2u_{i,j,k} + u_{i-1,j+1,k}) \\
& + \frac{c_{nn}}{2}(v_{i+1,j-1,k} - 2v_{i,j,k} + v_{i-1,j+1,k})
\end{aligned}
$$

$$+ \frac{c_{nn}}{2}(u_{i+1,j+1,k} - 2u_{i,j,k} + u_{i-1,j-1,k})$$

$$+ \frac{c_{nn}}{2}(v_{i+1,j+1,k} - 2v_{i,j,k} + v_{i-1,j-1,k})$$

$$+ \frac{c_{nn}}{2}(v_{i,j+1,k-1} - 2v_{i,j,k} + v_{i,j-1,k+1})$$

$$- \frac{c_{nn}}{2}(w_{i,j+1,k-1} - 2w_{i,j,k} + w_{i,j-1,k+1})$$

$$+ \frac{c_{nn}}{2}(v_{i,j+1,k+1} - 2v_{i,j,k} + v_{i,j-1,k-1})$$

$$+ \frac{c_{nn}}{2}(w_{i,j+1,k+1} - 2w_{i,j,k} + w_{i,j-1,k-1}), \quad (A3)$$

$$m\ddot{w}_{i,j,k} = c_n(w_{i,j,k+1} - 2w_{i,j,k} + w_{i,j,k-1})$$

$$- \frac{c_{nn}}{2}(u_{i+1,j,k-1} - 2u_{i,j,k} + u_{i-1,j,k+1})$$

$$+ \frac{c_{nn}}{2}(w_{i+1,j,k-1} - 2w_{i,j,k} + w_{i-1,j,k+1})$$

$$+ \frac{c_{nn}}{2}(u_{i+1,j,k+1} - 2u_{i,j,k} + u_{i-1,j,k-1})$$

$$+ \frac{c_{nn}}{2}(w_{i+1,j,k+1} - 2w_{i,j,k} + w_{i-1,j,k-1})$$

$$- \frac{c_{nn}}{2}(v_{i,j+1,k-1} - 2v_{i,j,k} + v_{i,j-1,k+1})$$

$$+ \frac{c_{nn}}{2}(w_{i,j+1,k-1} - 2w_{i,j,k} + w_{i,j-1,k+1})$$

$$+ \frac{c_{nn}}{2}(v_{i,j+1,k+1} - 2v_{i,j,k} + v_{i,j-1,k-1})$$

$$+ \frac{c_{nn}}{2}(w_{i,j+1,k+1} - 2w_{i,j,k} + w_{i,j-1,k-1}). \quad (A4)$$

The phonon dispersion relations are derived from the linearized equations of motion Eqs. (A2)–(A4). Solutions are sought in the form

$$u_{i,j,k} = U \exp[\mathrm{i}(qi + sj + pk - \omega t)],$$

$$v_{i,j,k} = V \exp[\mathrm{i}(qi + sj + pk - \omega t)], \quad (A5)$$

$$w_{i,j,k} = W \exp[\mathrm{i}(qi + sj + pk - \omega t)],$$

where i is imaginary unit; q, s, and p are the components of the wave vector; ω is frequency; and U, V, and W are the amplitudes.

Substituting Eq. (A5) into Eqs. (A2)–(A4), one can get

$$(m\omega^2 + P)U + QV + YW = 0,$$

$$QU + (m\omega^2 + Z)V + FW = 0, \quad (A6)$$

$$YU + FV + (m\omega^2 + S)W = 0,$$

where

$$P = -\alpha - \epsilon - \kappa - \eta - \xi,$$

$$Z = -\psi - \epsilon - \eta - \theta - \lambda,$$

$$S = -\delta - \kappa - \xi - \theta - \lambda,$$

$$Q = -\eta + \epsilon,$$

$$Y = -\xi + \kappa,$$

$$F = -\lambda + \theta, \quad (A7)$$

and

$$\alpha = 4c_n \sin^2 \frac{q}{2}, \quad \psi = 4c_n \sin^2 \frac{s}{2}, \quad \delta = 4c_n \sin^2 \frac{p}{2},$$

$$\epsilon = 2c_{nn} \sin^2 \frac{q-s}{2}, \quad \kappa = 2c_{nn} \sin^2 \frac{q-p}{2},$$

$$\eta = 2c_{nn} \sin^2 \frac{q+s}{2}, \quad \xi = 2c_{nn} \sin^2 \frac{q+p}{2},$$

$$\theta = 2c_{nn} \sin^2 \frac{s-p}{2}, \quad \lambda = 2c_{nn} \sin^2 \frac{s+p}{2}. \quad (A8)$$

A nonzero solution to the homogeneous system of linear equations Eq. (A6) in U, V, and W exists if and only if its determinant is equal to zero. From this condition, a cubic equation in ω^2 is obtained, which defines three branches of the dispersion relation,

$$m^3\omega^6 + (P + S + Z)m^2\omega^4$$

$$+ (PS + SZ + PZ - F^2 - Y^2 - Q^2)m\omega^2$$

$$+ 2FQY + PSZ - PF^2 - SQ^2 - ZY^2 = 0. \quad (A9)$$

[1] A. S. Dolgov, Sov. Phys. Solid State **28**, 907 (1986).

[2] A. J. Sievers and S. Takeno, Phys. Rev. Lett. **61**, 970 (1988).

[3] J. B. Page, Phys. Rev. B **41**, 7835 (1990).

[4] S. Flach and C. R. Willis, Phys. Rep. **295**, 181 (1998).

[5] D. K. Campbell, S. Flach, and Y. S. Kivshar, Phys. Today **57**(1), 43 (2004).

[6] S. Flach and A. V. Gorbach, Phys. Rep. **467**, 1 (2008).

[7] K. Ikeda, Y. Doi, B.-F. Feng, and T. Kawahara, Physica D **225**, 184 (2007).

[8] B.-F. Feng and T. Kawahara, Wave Motion **45**, 68 (2007).

[9] S. V. Dmitriev, E. A. Korznikova, J. A. Baimova, and M. G. Velarde, Phys.-Usp. **59**, 446 (2016).

[10] M. E. Manley, M. Yethiraj, H. Sinn, H. M. Volz, A. Alatas, J. C. Lashley, W. L. Hults, G. H. Lander, and J. L. Smith, Phys. Rev. Lett. **96**, 125501 (2006).

[11] M. E. Manley, J. W. Lynn, Y. Chen, and G. H. Lander, Phys. Rev. B **77**, 052301 (2008).

[12] M. E. Manley, A. J. Sievers, J. W. Lynn, S. A. Kiselev, N. I. Agladze, Y. Chen, A. Llobet, and A. Alatas, Phys. Rev. B **79**, 134304 (2009).

[13] A. J. Sievers, M. Sato, J. B. Page, and T. Rössler, Phys. Rev. B **88**, 104305 (2013).

[14] S. A. Kiselev and A. J. Sievers, Phys. Rev. B **55**, 5755 (1997).

[15] L. Z. Khadeeva and S. V. Dmitriev, Phys. Rev. B **81**, 214306 (2010).

[16] A. Rivière, S. Lepri, D. Colognesi, and F. Piazza, Phys. Rev. B **99**, 024307 (2019).

[17] N. K. Voulgarakis, G. Hadjisavvas, P. C. Kelires, and G. P. Tsironis, Phys. Rev. B **69**, 113201 (2004).

[18] R. T. Murzaev, D. V. Bachurin, E. A. Korznikova, and S. V. Dmitriev, Phys. Lett. A **381**, 1003 (2017).

[19] M. Haas, V. Hizhnyakov, A. Shelkan, M. Klopov, and A. J. Sievers, Phys. Rev. B **84**, 144303 (2011).

[20] A. Y. Morkina, D. V. Bachurin, S. V. Dmitriev, A. S. Semenov, and E. A. Korznikova, Materials **15**, 5597 (2022).

[21] I. D. Kolesnikov, S. A. Shcherbinin, Y. V. Bebikhov, E. A. Korznikova, I. A. Shepelev, A. A. Kudreyko, and S. V. Dmitriev, Chaos Soliton. Fract. **178**, 114339 (2024).

[22] O. V. Bachurina and A. A. Kudreyko, Comput. Mater. Sci. **182**, 109737 (2020).

[23] O. V. Bachurina, R. T. Murzaev, and D. V. Bachurin, J. Micromech. Mol. Phys. **4**, 1950001 (2019).

[24] O. V. Bachurina, Model. Simul. Mater. Sci. Eng. **27**, 055001 (2019).

[25] O. V. Bachurina, Comput. Mater. Sci. **160**, 217 (2019).

[26] O. V. Bachurina and A. A. Kudreyko, Eur. Phys. J. B **94**, 218 (2021).

[27] K. A. Krylova, I. P. Lobzenko, A. S. Semenov, A. A. Kudreyko, and S. V. Dmitriev, Comput. Mater. Sci. **180**, 109695 (2020).

[28] R. T. Murzaev, A. A. Kistanov, V. I. Dubinko, D. A. Terentyev, and S. V. Dmitriev, Comput. Mater. Sci. **98**, 88 (2015).

[29] Y. Doi, T. Komiya, S. Nagashima, and A. Nakatani, Zairyo **70**, 330 (2021).

[30] O. V. Bachurina, R. T. Murzaev, A. A. Kudreyko, S. V. Dmitriev, and D. V. Bachurin, Eur. Phys. J. B **95**, 104 (2022).

[31] O. V. Bachurina, R. T. Murzaev, A. S. Semenov, E. A. Korznikova, and S. V. Dmitriev, Phys. Solid State **60**, 989 (2018).

[32] R. T. Murzaev, R. I. Babicheva, K. Zhou, E. A. Korznikova, S. Y. Fomin, V. V. Dubinko, and S. V. Dmitriev, Eur. Phys. J. B **89**, 168 (2016).

[33] N. N. Medvedev, M. D. Starostenkov, and M. E. Manley, J. Appl. Phys. **114**, 213506 (2013).

[34] N. N. Medvedev, M. D. Starostenkov, P. V. Zakharov, and O. Pozidaeva, Tech. Phys. Lett. **37**, 98 (2011).

[35] P. V. Zakharov, E. A. Korznikova, S. V. Dmitriev, E. G. Ekomasov, and K. Zhou, Surf. Sci. **679**, 1 (2019).

[36] R. Haque, M. Sekh, G. Kibria, and S. Haidar, Facta Univ., Ser.: Mech. Eng. **21**, 063 (2023).

[37] A. V. Savin and S. V. Dmitriev, Phys. Rev. E **107**, 054216 (2023).

[38] L. Z. Khadeeva and S. V. Dmitriev, Phys. Rev. B **84**, 144304 (2011).

[39] E. A. Korznikova, S. Y. Fomin, E. G. Soboleva, and S. V. Dmitriev, JETP Lett. **103**, 277 (2016).

[40] Y. Yamayose, Y. Kinoshita, Y. Doi, A. Nakatani, and T. Kitamura, Europhys. Lett. **80**, 40008 (2007).

[41] V. Hizhnyakov, M. Klopov, and A. Shelkan, Phys. Lett. A **380**, 1075 (2016).

[42] A. Fraile, E. Koukaras, K. Papagelis, N. Lazarides, and G. Tsironis, Chaos, Soliton. Fract. **87**, 262 (2016).

[43] Y. Doi and A. Nakatani, Procedia Eng. **10**, 3393 (2011).

[44] G. M. Chechin, S. V. Dmitriev, I. P. Lobzenko, and D. S. Ryabov, Phys. Rev. B **90**, 045432 (2014).

[45] K. A. Krylova, J. A. Baimova, R. T. Murzaev, and R. R. Mulyukov, Phys. Lett. A **383**, 1583 (2019).

[46] A. V. Savin, E. A. Korznikova, and S. V. Dmitriev, J. Sound Vib. **520**, 116627 (2022).

[47] Y. Kinoshita, Y. Yamayose, Y. Doi, A. Nakatani, and T. Kitamura, Phys. Rev. B **77**, 024307 (2008).

[48] T. Shimada, D. Shirasaki, and T. Kitamura, Phys. Rev. B **81**, 035401 (2010).

[49] T. Shimada, D. Shirasaki, Y. Kinoshita, Y. Doi, A. Nakatani, and T. Kitamura, Physica D **239**, 407 (2010).

[50] J. Cuevas, J. F. R. Archilla, B. Sánchez-Rey, and F. R. Romero, Physica D **216**, 115 (2006).

[51] D. A. Terentyev, A. V. Dubinko, V. I. Dubinko, S. V. Dmitriev, E. E. Zhurkin, and M. V. Sorokin, Modelling Simul. Mater. Sci. Eng. **23**, 085007 (2015).

[52] J. A. Baimova, R. T. Murzaev, and A. I. Rudskoy, Phys. Lett. A **381**, 3049 (2017).

[53] M. E. Manley, Acta Mater. **58**, 2926 (2010).

[54] V. I. Dubinko, P. A. Selyshchev, and J. F. R. Archilla, Phys. Rev. E **83**, 041124 (2011).

[55] D. Xiong, J. Wang, Y. Zhang, and H. Zhao, Phys. Rev. E **85**, 020102 (2012).

[56] E. A. Korznikova, A. Y. Morkina, M. Singh, A. M. Krivtsov, V. A. Kuzkin, V. A. Gani, Y. V. Bebikhov, and S. V. Dmitriev, Eur. Phys. J. B **93**, 123 (2020).

[57] A. Upadhyaya, M. N. Semenova, A. A. Kudreyko, and S. V. Dmitriev, Commun. Nonlinear Sci. **112**, 106541 (2022).

[58] M. Singh, A. Y. Morkina, E. A. Korznikova, V. I. Dubinko, D. A. Terentiev, D. Xiong, O. B. Naimark, V. A. Gani, and S. V. Dmitriev, J. Nonlinear Sci. **31**, 12 (2021).

[59] V. M. Burlakov, S. A. Kiselev, and V. I. Rupasov, Phys. Lett. A **147**, 130 (1990).

[60] T. Dauxois, R. Khomeriki, F. Piazza, and S. Ruffo, Chaos **15**, 015110 (2005).

[61] I. Daumont, T. Dauxois, and M. Peyrard, Nonlinearity **10**, 617 (1997).

[62] K. Yoshimura, Phys. Rev. E **70**, 016611 (2004).

[63] Y. A. Kosevich and S. Lepri, Phys. Rev. B **61**, 299 (2000).

[64] B. Tang and K. Deng, Nonlinear Dyn. **88**, 2417 (2017).

[65] L. Kavitha, A. Mohamadou, E. Parasuraman, D. Gopi, N. Akila, and A. Prabhu, J. Magn. Magn. Mater. **404**, 91 (2016).

[66] L. Kavitha, E. Parasuraman, D. Gopi, A. Prabhu, and R. Vicencio, J. Magn. Magn. Mater. **401**, 394 (2016).

[67] E. A. Korznikova, D. V. Bachurin, S. Y. Fomin, A. P. Chetverikov, and S. V. Dmitriev, Eur. Phys. J. B **90**, 23 (2017).

[68] R. I. Babicheva, A. S. Semenov, E. G. Soboleva, A. A. Kudreyko, K. Zhou, and S. V. Dmitriev, Phys. Rev. E **103**, 052202 (2021).

[69] E. K. Naumov, Y. V. Bebikhov, E. G. Ekomasov, E. G. Soboleva, and S. V. Dmitriev, Phys. Rev. E **107**, 034214 (2023).

[70] G. M. Chechin, G. S. Dzhelauhova, and E. A. Mehonoshina, Phys. Rev. E **74**, 036608 (2006).

[71] G. M. Chechin and V. P. Sakhnenko, Physica D **117**, 43 (1998).

[72] D. S. Ryabov, G. M. Chechin, E. K. Naumov, Y. V. Bebikhov, E. A. Korznikova, and S. V. Dmitriev, Nonlinear Dyn. **111**, 8135 (2023).

[73] D. S. Ryabov, G. M. Chechin, A. Upadhyaya, E. A. Korznikova, V. I. Dubinko, and S. V. Dmitriev, Nonlinear Dyn. **102**, 2793 (2020).

[74] I. V. Kosarev, S. A. Shcherbinin, A. A. Kistanov, R. I. Babicheva, E. A. Korznikova, and S. V. Dmitriev, Comp. Mater. Sci. **231**, 112597 (2023).

[75] R. I. Babicheva, A. S. Semenov, S. A. Shcherbinin, E. A. Korznikova, A. A. Kudreyko, P. Vivegananthan, K. Zhou, and S. V. Dmitriev, Phys. Rev. E **105**, 064204 (2022).

[76] S. A. Shcherbinin, K. A. Krylova, G. M. Chechin, E. G. Soboleva, and S. V. Dmitriev, Commun. Nonlinear Sci. **104**, 106039 (2022).

[77] G. Chechin, D. Ryabov, and S. Shcherbinin, Phys. Rev. E **92**, 012907 (2015).

[78] G. M. Chechin, N. V. Novikova, and A. A. Abramenko, Physica D **166**, 208 (2002).

[79] G. M. Chechin, D. S. Ryabov, and S. A. Shcherbinin, Lett. Mater. **6**, 9 (2016).

[80] G. Chechin, D. Ryabov, and S. Shcherbinin, J. Micromech. Mol. Phys. **03**, 1850002 (2018).

[81] G. Chechin and D. Ryabov, Commun. Nonlinear Sci. **120**, 107176 (2023).

[82] A. Khater, R. Tigrine, and B. Bourahla, Phys. Status Solidi B **246**, 1614 (2009).

[83] A. Zaoui, A. Belabbes, R. Ahuja, and M. Ferhat, Phys. Lett. A **375**, 1695 (2011).

[84] A. Belabbes, A. Zaoui, and M. Ferhat, Solid State Commun. **150**, 2337 (2010).

[85] C.-J. Kang, K. Kim, and B. I. Min, Phys. Rev. B **86**, 054115 (2012).

[86] J. Dorignac, J. Zhou, and D. K. Campbell, Physica D **237**, 486 (2008).

[87] N. S. Bakhvalov, *Numerical Methods: Analysis, Algebra, Ordinary Differential Equations* (MIR Publishers, Moscow, 1977).

[88] A. Gimenez, V. Chausse, and A. Meseguer, Eur. J. Phys., **36**, 015015 (2014).

[89] L. Chen and B. Basu, Appl. Ocean Res. **111**, 102631 (2021).

[90] V. L'opez, Commun. Nonlinear Sci. **61**, 248 (2018).

[91] D. Amann and K. Kalimeris, Eur. J. Mech. B - Fluid. **67**, 314 (2018).